Eur. Phys. J. D **32**, 329–337 (2005)
DOI: 10.1140/epjd/e2005-00026-8

THE EUROPEAN PHYSICAL JOURNAL D

A density functional study of small Al_xO_y (x, y = 1−4) clusters and their thermodynamic properties

A.B.C. Patzer[a], Ch. Chang, E. Sedlmayr, and D. Sülzle

Zentrum für Astronomie und Astrophysik, Technische Universität Berlin, Hardenbergstr. 36, 10623 Berlin, Germany

Received 17 May 2004 / Received in final form 7 July 2004
Published online 15 February 2005 –

Abstract. We report thermodynamic properties of small aluminium oxide clusters of mixed stoichiometric ratio Al_xO_y ($x, y = 1-4$). The rigid rotator-harmonic oscillator approximation is used to calculate the partition function as it is generally applied in thermodynamic studies of polyatomic molecules. The molecular data used to set up the partition functions were computed by density functional techniques employing the BP86 gradient corrected exchange correlation functional. Thereby, the results of three species viz. AlO_4, Al_4O_2, and Al_4O_3 previously not reported in the literature are included in this study. Equilibrium geometric parameters, energies, selected harmonic vibrational wave numbers of energetically low–lying stationary points are presented along with corresponding absorption coefficients. The resulting thermodynamic functions of aluminium oxides are consistent with the JANAF thermochemical data compilation. These functions are used to determine the temperature dependent chemical equilibrium partial pressure distributions for different aluminium to oxygen ratios.

PACS. 33.15.-e Properties of molecules – 82.60.-s Chemical thermodynamics

1 Introduction

Thermodynamic data are required for many investigations as, for example, the study of gas phase chemistry or modelling processes in stellar atmospheres. Unfortunately for many relevant molecules this information is still unavailable. Theoretical computation is therefore often the only means to obtain at least some estimates of the desired quantities.

First candidates to play an important role in dust condensation processes from the gas phase in oxygen–rich astrophysical environments are inorganic materials such as the oxides of those chemical elements showing sufficient abundances and a bulk phase which is usually characterised by elevated melting points and hence high energetic stability (e.g. Gail and Sedlmayr [1]). Among other oxygen bearing compounds aluminium oxides are possible candidates that could be involved in such processes [2–5]; but merely data for the smallest cluster sizes ($x, y = 1-2$) are available [6]. The availability of adequate thermochemical data for Al_xO_y species in the gas phase is not only needed for astrophysical applications but also, for example, for the study of evaporation processes in Al–O–systems [7–9] important to ceramic and material sciences.

There is extensive literature on small Al_xO_y ($x, y \leq 3$) systems as well as on Al_4O, Al_2O_4, Al_3O_4, and Al_4O_4 reporting theoretical electronic structure investigations at various different levels of theory [10–28]. In this contribution, the nature and physical properties of all aluminium oxide clusters of mixed stoichiometric ratio up to the tetramer of the AlO molecule have been studied theoretically employing computational electronic structure density functional techniques. Thereby, we additionally present the results of three species hitherto not reported in the literature viz. AlO_4, Al_4O_2, and Al_4O_3. In the following the molecular data of all these theoretical investigations are used to derive the thermodynamic functions for these Al_xO_y molecules in the gas phase adhering rigorously to the JANAF reference system [6]. The properties, thus obtained, are necessary prerequisites for the study of phase transitions in oxygen–rich (astro–)physical environments.

2 Computational remarks

2.1 DFT calculations

All aluminium oxide clusters were treated within a density functional approach by full optimisation and characterisation of the stationary points at the DFT/BP86 [29–31] level of theory in various spin states in conjunction with the standard medium sized all–electron split valence 6–31G(d) basis set [32]. In view of a consistent level of description for all Al_xO_y clusters for even much larger cluster sizes this level of approximation is a reasonable

[a] e-mail: patzer@astro.physik.tu-berlin.de

compromise between computational effort and desired accuracy with regard to atomisation energies as demonstrated by the comparative study of different computational approaches for the electronic structure properties of the Al_4O_4 molecular system [28]. Thus, the ultimate intention of this study was not to perform calculations at the most elaborate level of theory available, which for systems of relatively small sizes are still feasible. The wavenumbers $\tilde{\nu}$ of the vibrations are computed in the harmonic approximation, from which the zero point vibrational energies E_{zp} can be calculated. Additionally the integrated absorption coefficients A_k for strictly harmonic motion are obtained from the corresponding normal coordinate of the kth vibrational mode and the electric dipole moment. The atomisation energies D_{at} are calculated form the determined total electronic energies E_{tot} of the cluster and the separated atoms in their electronic ground states. All DFT computations were performed with help of the GAUSSIAN system of programs [33].

2.2 Thermochemistry

In order to obtain the thermodynamic functions of Al_xO_y clusters that are consistent with the JANAF data compilation we used the JANAF thermochemical reference system for an ideal gas at standard pressure $p^{\ominus} = 1$ bar and reference temperature $T_0 = 298.15$ K (see Chase [6] for details). All values were calculated using a consistent set of auxiliary data taken from the JANAF tables [6]. In this way the calculated heats of formation at $T = 0$ K, $\Delta_f H^{\ominus}(0)$, were obtained from the theoretical atomisation enthalpies $\Delta_{at}H$ in conjunction with the standard experimental $\Delta_f H^{\ominus}(0)$ values for the neutral atoms.

The rigid rotator-harmonic oscillator (RRHO) approximation is used to set up the partition function as it is generally applied in thermodynamic studies of polyatomic molecules. From the partition function the thermodynamic functions like the entropy $S^{\ominus}(T)$, the standard enthalpy of formation $\Delta_f H^{\ominus}(T)$, the Gibbs energy of formation $\Delta_f G^{\ominus}(T)$, and the heat capacities $C^{\ominus}{}_p(T)$ can easily be calculated by standard statistics as described by e.g. Hill [34].

3 Results and discussion

3.1 DFT results

Each aluminium oxide cluster system Al_xO_y so far considered discloses an amazingly rich structural diversity of energetically low–lying, highly stable isomers as well as charge and spin states. In particular the species with $x, y \leq 2$, the atomisation energies D_0 of which are known experimentally [6] serve as a means to assess the quality of the employed approach. The most stable configuration of all discussed Al_xO_y clusters[1] computed by this DFT approach are depicted in Figure 1. The corresponding electronic states and point groups are also indicated.

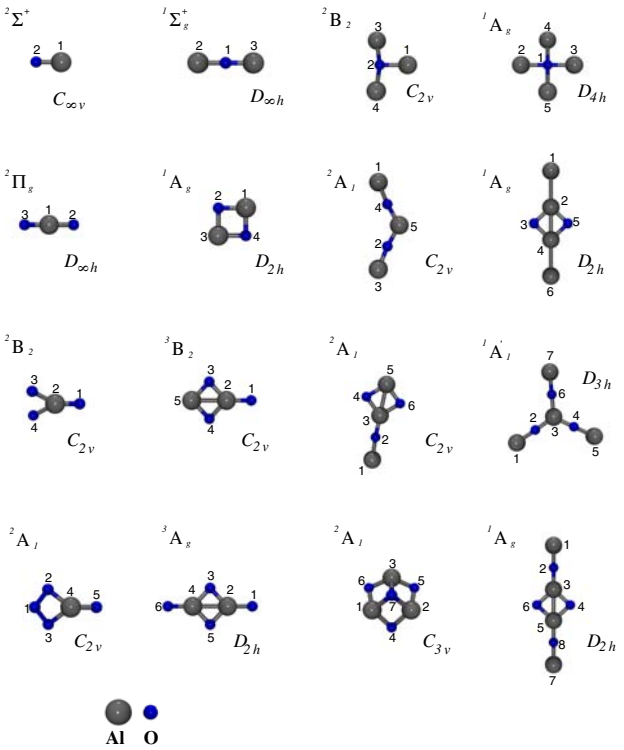

Fig. 1. DFT/BP86/6–31G(d) geometries of the energetically lowest aluminium oxide isomers. Point groups and electronic states are also indicated.

The cluster structures seem to be preferably planar. If permitted by the given ratio (x/y), aluminium atoms tend to have at most three nearest neighbours, preferably oxygen. Oxygen atoms on the other hand have at most two nearest neighbours, preferably aluminium. Therefore, the geometrical arrangements are mainly planar patterns of alternating Al and O atoms. Most conspicuous in many configurations is a recurring pattern of a rhombic $(AlO)_2$ unit.

A first exception to this behaviour is the molecular system Al_3O_4. The energetically lowest structure has a three–dimensional pyramidal (C_{3v}) geometry with a perfectly threefold coordinated oxygen atom at the top. The isomer having the expected planar geometric arrangement represents a stable energetic configuration as well, but its binding energy is by about 1.4 eV smaller (see also Martinez et al. [26][2]).

Because of the unanticipated geometry of the energetically lowest Al_3O_4 isomer, a more particularised study of this structure seemed to be justified. It is interesting to note that according to our studies the energetic order of these two configurations can be equally established at various other levels of theory (e.g. MP2/6–31G(d), QCISD/6–31G(d)), but it is inverted upon the orthodox

[1] Note, that the linear singlet Al_2O_3 isomer being of comparable stability [27] is not discussed in the following.

[2] The planar arrangement involving the rhombic $(AlO)_2$–unit is indeed the ground state structure of the negative ion $Al_3O_4^-$ [26].

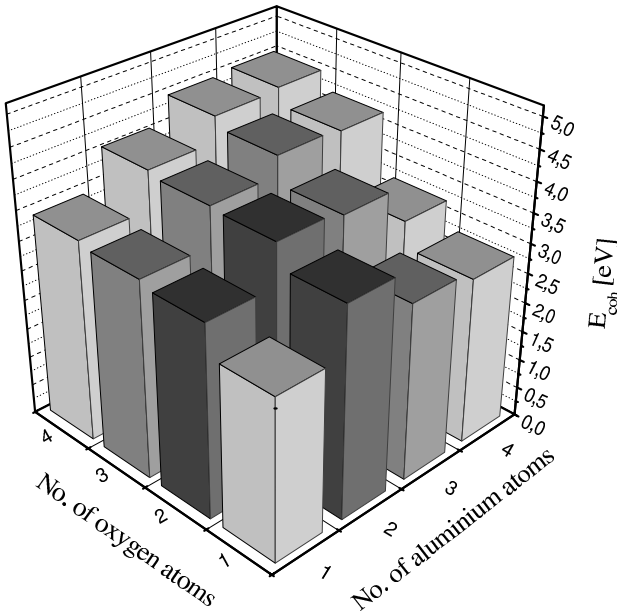

Fig. 2. DFT/BP86/6–31G(d) cohesive energies.

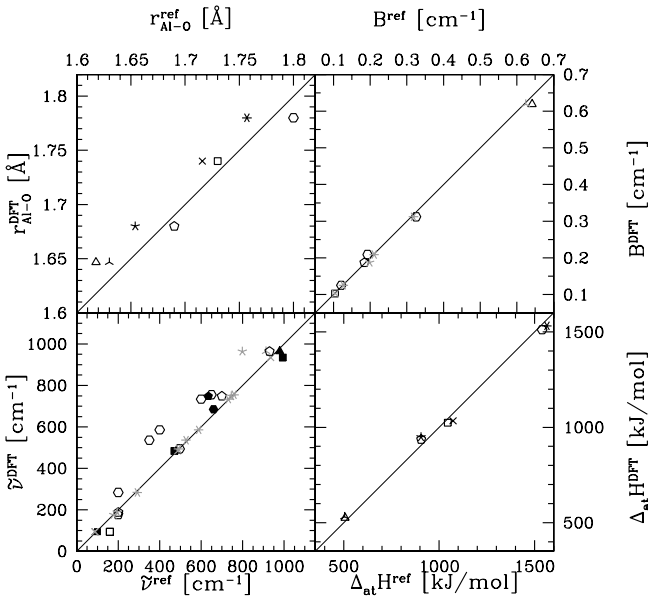

Fig. 3. Comparison of AlO (triangles), Al_2O (squares), AlO_2 (pentagons), Al_2O_2 (hexagons) DFT/BP86/6–31G(d) properties with corresponding data used in Chase [6] (unfilled symbols). In addition, the DFT frequencies are compared with other experimental values (filled symbols) taken from [37–40]. The crosses mark the analogous comparison with recent theoretical results (Ref. [21] – (black), Ref. [20] – (grey)).

Hartree Fock (HF) and also a restricted multiconfigurational CASSCF approach. This clearly indicates that a sufficiently correlated level of theory is coercively necessary to adequately treat these kind of molecular species.

The binding energy per atom, the cohesive energy E_{coh}, of the aluminium–oxygen clusters Al_xO_y ($x, y = 1-4$) depicted in Figure 1 resulting from the DFT/BP86/6–31G(d) calculations is graphically shown in Figure 2. The energetically most stable species tend to lie along the diagonal ($x = y$) or in close vicinity to it. The binding energy per atom E_{coh} increases in this direction. Systems which have an excess of oxygen ($y > x$) are obviously more favourable than those with more aluminium atoms ($y < x$).

All IR active lines of these small aluminium oxide clusters are distributed within the interval of (150–1050 cm^{-1}); many of them are located at the upper end around 1000 cm^{-1}, where several spectral lines have been experimentally observed [35]. The most prominent feature lies at 1012 cm^{-1} (Al_4O_4) [28].

In order to assess the quality of the employed computational approach the relevant molecular properties of species with $x, y \leq 2$ computed at the DFT/BP86/6–31G(d) level of theory are compared with known experimental data and recent theoretical results as illustrated by Figure 3. Except for the diatomic molecule our findings agree remarkably with those data and even the results obtained for AlO are in reasonable agreement with the experimental values ([36]). The DFT/BP86/6–31G(d) atomisation energies of the larger molecules and the JANAF data match within the error bars given in Chase [6]. Only Al_2O shows a somewhat larger deviation of 0.05 eV. The Al–O bond lengths exhibit an average deviation from the values adopted in the thermochemical tables of 0.8%. The comparison between the DFT/BP86/6–31G(d) vibrational frequencies and the roughly estimated values given in Chase [6] reveals noticeable discrepancies. However, our results are in rather good agreement with other experimental data [37–40].

A comparison of our findings with two of the most recent theoretical contributions (cf. Fig. 3) shows that the average deviation of the BP86/6–31G(d) energies and those obtained by the more expensive CBS–QB3 approach [21] is about 0.4 eV[3], whereas their Al–O bond distances are systematically smaller by ∼0.022 Å. The DFT rotational constants resulting from two different functionals (BP86, B3LYP) are in very good agreement, which is, in principle, equally true for the frequencies except for the largest AlO_2 vibration[4]. However, Swihart et al. [20] had to artificially scale their B3LYP values.

Table 1 summarises and compares the energies of atomisation of the energetically lowest isomers of those small Al_xO_y species that have been already reported in the literature and for which no experimental results are available. It is obvious that the DFT/BP86/6–31G(d) level of approximation is again well in line with those approaches employing more elaborate techniques and/or very large

[3] Note, that the comparison of the theoretical energies does not involve zero point energies due to the lack of data given in [21].

[4] We also observed the spin contamination effect mentioned by [20] for the AlO_2 singlet. But in addition, we detected another minimum on this singlet potential energy surface (PES), 1.06 eV higher in energy, which has also a linear configuration with a shorter Al–O bond length (0.037 Å) but without showing any spin contamination. The nature of the very complex PES of the AlO_2 system is discussed by [19].

Table 1. Comparison of DFT/BP86/6–31G(d) atomisation energies of Al_3O, AlO_3, Al_2O_3, Al_3O_2, Al_3O_3, Al_2O_4, Al_4O, Al_3O_4 with former results 1: this work, 2: reference [21], 3: references [17,18].

	$\langle\hat{S}^2\rangle$ BP86 6–31G(d)[1]	D_{at}[eV] BP86 6–31G(d)[1]	D_{at}[eV] CBS–QB3[2]	D_{at}[eV] CCSD(T) 6–31G(d)[3]
Al_3O	0.76	12.00	11.24[a]	11.14
AlO_3	0.75	13.32	12.81	
Al_2O_3	2.00	20.08	20.43	
Al_3O_2	0.75	19.36	20.09	18.90
Al_3O_3	0.75	26.01	26.94	25.22
Al_2O_4	2.01	24.56	25.04	23.01[b]
Al_4O	0.00	14.19	13.23[a]	
Al_3O_4	0.76	31.61	30.49[c]	

[a] PMP4(SDTQ)/6–311G* values [12].
[b] CCSDT/6-311G** value [15].
[c] B3LYP/6-311+G(2d) value [26].

Table 2. DFT/BP86/6-31G(d) equilibrium geometric parameters of Al_3O, AlO_3, Al_2O_3, Al_3O_2, Al_3O_3, Al_2O_4, Al_4O, Al_3O_4. The geometric meaning of the interatomic distances r_{ij}/Å, angles α_{ijk}/deg, and dihedral angles δ_{ijkl}/deg can be inferred from Figure 1.

Al_3O	$r_{12} = 1.977$	$r_{23} = 1.854$	
	$\alpha_{324} = 166.4$		
AlO_3	$r_{12} = 1.623$	$r_{23} = 1.881$	
	$\alpha_{324} = 43.6$		
Al_2O_3	$r_{12} = 1.750$	$r_{24} = 1.764$	$r_{45} = 1.788$
	$\alpha_{354} = 92.9$	$\alpha_{324} = 94.6$	
Al_3O_2	$r_{12} = 1.730$	$r_{23} = 1.733$	
	$\alpha_{123} = 172.6$	$\alpha_{234} = 122.0$	
Al_3O_3	$r_{12} = 1.736$	$r_{23} = 1.705$	$r_{34} = 1.772$
	$r_{46} = 1.784$		
	$\alpha_{123} = 180.0$	$\alpha_{465} = 93.7$	$\alpha_{435} = 94.5$
Al_2O_4	$r_{12} = 1.763$	$r_{24} = 1.771$	
	$\alpha_{324} = 94.1$		
Al_4O	$r_{12} = 2.797$	$r_{15} = 1.978$	
	$\alpha_{123} = 90.0$		
Al_3O_4	$r_{12} = 2.497$	$r_{14} = 1.782$	$r_{17} = 1.897$
	$\delta_{1235} = 149.6$		

basis sets. This equally applies to the geometric configurations which are quantitatively given in Table 2 for this level of theory. Their vibrational wave numbers $\tilde{\nu}_k$ and the related integrated absorption coefficients A_k are listed in Table 3. Detailed information about the tetramer is particularised for several levels of theory in Chang et al. [28].

The geometric arrangements of the energetically lowest isomer of the species AlO_4, Al_4O_2, and Al_4O_3 fit well into this general building scheme of a preferred planarity and a tendency to form patterns of alternating Al and O atoms if structurally possible see Figure 1. The corresponding geometric parameters are given in Table 4 and their vibrational wave numbers as well as the corresponding integrated absorption coefficients are tabulated in Table 5. The details about the energetics of these three species are listed in Table 6. It is commonly known, that DFT calculations may suffer from spin symmetry breaking for open shell systems. However, the BP86/6–31G(d) values for $\langle\hat{S}^2\rangle$ as given in Tables 1 and 6 indicate, that symmetry breaking remains marginal in these cases. This is equally true for the states of the free atoms (Al(^2P), $\langle\hat{S}^2\rangle = 0.75$, O($^3P$), $\langle\hat{S}^2\rangle = 2.00$) required for the determination of the atomisation energies.

Table 3. Harmonic wave numbers $\tilde{\nu}$ and integrated IR absorption coefficients A_k (DFT/BP86/6–31G(d)) of AlO_3, Al_3O, Al_4O, Al_3O_2, Al_2O_3, Al_2O_4, Al_3O_3, Al_3O_4. Only $A_k > 50 \times 10^{-8}$ cm^{-2} s^{-1} are given in parentheses.

	$\tilde{\nu}_k$[cm^{-1}] (A_k[10^{-8} cm^{-2}s^{-1}])
AlO_3	173 175 464 536 1045 1111
Al_3O	143 148 167 347 434 619
Al_4O	88 133 197 207 207 250 373 505(96) 505(96)
Al_3O_2	47 75 87 89 220 448 558 955 974(446)
Al_2O_3	54 162 299 398 594 615(68) 686 734(55) 855
Al_2O_4	58 144 172 196 322(59) 349 591 601 622 751(85) 824 868
Al_3O_3	31 41 147 147 209 331 333 565 601 701(79) 740(57) 767 1031(318)
Al_3O_4	224 225 305 319 320 479 480 532 541 542 634 664 679 774 774

Table 4. DFT/BP86/6-31G(d) equilibrium geometric parameters of AlO_4, Al_4O_2, Al_4O_3. The geometric meaning of the interatomic distances r_{ij}/Å and angles α_{ijk}/deg can be inferred from Figure 1.

AlO_4	$r_{12} = 1.421$	$r_{24} = 1.845$	$r_{45} = 1.660$
	$\alpha_{213} = 105.6$	$\alpha_{243} = 75.7$	
Al_4O_2	$r_{12} = 2.804$	$r_{23} = 1.790$	
	$\alpha_{345} = 93.1$		
Al_4O_3	$r_{12} = 1.728$	$r_{23} = 1.781$	
	$\alpha_{234} = 120$		

Table 5. Harmonic wave numbers $\tilde{\nu}$ and integrated IR absorption coefficients A_k (DFT/BP86/6–31G(d)) of AlO_4, Al_4O_2, Al_4O_3. Only $A_k > 50 \times 10^{-8}$cm^{-2} s^{-1} are given in parentheses.

	$\tilde{\nu}_k$[cm^{-1}] (A_k[10^{-8} cm^{-2} s^{-1}])
AlO_4	149 168 291 411 534 746 809 862(65) 1008
Al_4O_2	25 32 65 74 183 242 261 516 579 690(274) 714(51) 750
Al_4O_3	29 31 40 54 71 73 247 247 299 341 587 587 998 1019(451) 1019(451)

3.2 Thermochemical functions

The molecular data of all these theoretical investigations are now used to derive the related thermodynamic functions for the Al_xO_y ($x, y = 1$–4) molecules in the gas phase adhering rigorously to the JANAF reference system [6], in order to avoid errors due to a lack of consistency between thermodynamic data from different compilations or sources, which are mainly caused by differences in the reference systems used (e.g. reference state of the elements, standard pressure $p^{\ominus}$, or reference temperature T_0).

Table 6. DFT/BP86/6-31G(d) energies of AlO_4, Al_4O_2, Al_4O_3.

	E_{tot}^{BP86}[Hartree]	E_{zp}[eV]	D_{at}[eV]	$\langle\hat{S}^2\rangle$
AlO_4	–543.20252457	0.31	17.33	0.76
Al_4O_2	–1120.27988590	0.26	19.63	0.00
Al_4O_3	–1195.70722158	0.35	29.89	0.00

Table 7. Comparison of calculated enthalpies of formation at reference temperature T_0 = 298.15 K based on different theoretical approaches.

	$\Delta_f H^\circ(T_0)$ [kJ mol^{-1}]				
	B3LYP[a]	G2[a]	CBS–Q[a]	CBS–QB3[b]	BP86[c]
AlO_2	–56.1	–42.7	–66.5	–69.5	–116.8
Al_2O	–118.0	–149.0	–161.9	–162.3	–123.1
Al_2O_2	–309.6	–367.8	–395.4	–395.4	–368.4
Al_2O_3				–546.4	–521.2
AlO_3				–143.9	–220.9
Al_3O_2				–436.8	–372.8
Al_3O_3				–840.6	–759.5
Al_2O_4				–735.5	–701.1

[a] reference [20], [b] reference [21], [c] this work.

According to the JANAF style we calculated the thermodynamic functions from 100 K to 3000 K temperature range in increments of 100 K. The different contributions to the partition function, from which the thermodynamic functions can easily be calculated by standard statistics, were evaluated separately. The required data to set up the electronic, rotational, and vibrational partition functions are given in the Tables 1–6 and Figure 1.

To compare the obtained results with data reported in the literature, calculated enthalpies of formation $\Delta_f H^\circ(T_0)$ based on different theoretical methods are listed in Table 7 for several aluminium oxide clusters. Our $\Delta_f H^\circ(T_0)$ value of AlO_2 is noticeable lower than the other theoretical results. But it is more in agreement with the experimental data given in JANAF (–86 kJ/mol) or in Lias et al. [41] (–130 kJ/mol), which is even lower. The same can be observed for the molecule even richer in oxygen, AlO_3, for which the BP86 $\Delta_f H^\circ(T_0)$ is also clearly lower than the corresponding CBS–QB3 value. The results for Al_2O and Al_2O_2 are quite in line with those obtained by the other four approaches and with the JANAF data. The data given by Politzer et al. [21] for Al_2O_3 and Al_2O_4 are in reasonable agreement with our results, whereas the less oxygen containing species Al_3O_2 and Al_3O_3 show quite pronounced deviations. These discrepancies are mainly caused by the differences in the D_{at} values (cf. Tab. 1). However, the results computed by Ghanty and Davidson [17,18], which employ a rather elaborate computational method (CCSD(T)), indicate to favour smaller D_{at} values.

A list of all thermochemical functions namely entropies, enthalpies of formation, and Gibbs potentials at reference temperature T_0 = 298.15 K based on DFT/BP86/6–31G(d) results is given in Table 8 for the larger aluminium oxide clusters.

Table 8. Entropies, enthalpies of formation, and Gibbs potentials at reference temperature T_0 based on DFT/BP86/6–31G(d) results.

	$S^\circ(T_0)$ [J (mol K)$^{-1}$]	$\Delta_f H^\circ(T_0)$ [kJ mol^{-1}]	$\Delta_f G^\circ(T_0)$ [kJ mol^{-1}]
AlO_3	289.6	–220.9	–207.1
AlO_4	309.2	–333.5	–294.9
Al_2O_3	327.0	–521.2	–510.1
Al_2O_4	348.5	–701.1	–665.9
Al_3O	321.5	81.0	41.0
Al_3O_2	368.2	–372.8	–396.1
Al_3O_3	371.7	–759.5	–753.3
Al_3O_4	336.9	–1079.0	–1031.8
Al_4O	341.0	200.1	162.8
Al_4O_2	398.4	–68.4	–92.2
Al_4O_3	442.4	–802.6	–809.0
Al_4O_4	446.1	–1181.7	–1158.6

Table 9. Fit coefficients (cf. Eq. (1)) for the C_p values of molecular Al_xO_y clusters in the temperature range between T_0 and 3000 K based on DFT/BP86/6–31G(d) results.

	a	b	c	d
AlO_3	74.5883	7.11721	–1.34670	–1.51299
AlO_4	98.5352	8.05461	–2.18922	–1.72620
Al_2O_3	101.672	5.45730	–2.07312	–1.17566
Al_2O_4	124.877	6.92482	–2.50008	–1.49040
Al_3O	81.9689	1.00842	–0.767551	–0.218348
Al_3O_2	101.316	5.68705	–1.39446	–1.21596
Al_3O_3	123.803	7.79673	–2.46049	–1.67294
Al_3O_4	149.256	7.44435	–3.57734	–1.60736
Al_4O	107.050	0.894055	–0.954005	–0.194089
Al_4O_2	127.960	4.32524	–1.87464	–0.933352
Al_4O_3	146.393	9.69496	–2.22341	–2.06886
Al_4O_4	168.993	11.7167	–3.19367	–2.50800

The values of the thermodynamic functions at other temperatures can be obtained from the heat capacities C°_p. Their temperature dependence can be described by a polynomial fit as used by e.g. Binnewies and Milke [42]

$$C^\circ_p(T) = a + b\times\left(\frac{T}{10^3}\right) + c\times\left(\frac{T}{10^3}\right)^{-2} + d\times\left(\frac{T}{10^3}\right)^{2}. \quad (1)$$

The corresponding fit coefficients of the molecular Al_xO_y clusters in the temperature range between T_0 and 3000 K are given in Table 9.

The connection of the molar Gibbs free energy of formation to the cluster stoichiometry can clearly be seen in Figure 4, which illustrates the size and temperature dependence of $\Delta_f G^\circ$ of the main isomers of mixed stoichiometric ratio Al_xO_y. At each temperature the $\Delta_f G^\circ$ values of the $(AlO)_x$ clusters are generally the lowest. There are only two exceptions namely Al_2O and for low temperatures also Al_3O_4. Both are probably related to changes in the dimension of the clusters, i.e. in case of Al_2O (Al_3O_4) the cluster structure changes from linear

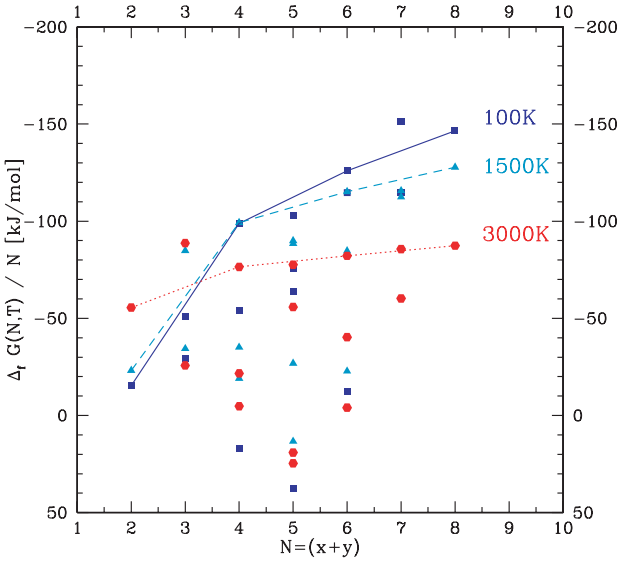

Fig. 4. Size dependence of $\Delta_f G$ of the main isomers of mixed stoichiometric ratio Al_xO_y $(x, y = 1{-}4)$ normalised to the number of atoms $N = x + y$ in the cluster at $T = 2000$ K (dotted line, hexagons), $T = 1000$ K (dashed line, triangle), and $T = 500$ K (solid line, squares). The three lines connect the data of the $(AlO)_x$, $x = 1{-}4$ clusters.

(planar) to planar (three dimensional). However, $(AlO)_x$ is the preferred cluster stoichiometry in this cluster size regime especially at high temperatures.

4 Application: multicomponent gas phase dissociative equilibrium

The availability of thermodynamic functions for molecular systems is of determinative importance for the calculation of multicomponent gas phase equilibria. If a gaseous system at temperature T and pressure P consisting of, for instance, N_S elements $A, B, C, \cdots, S$ is envisaged, then by the law of mass conservation and the condition that the Gibbs free energy is minimal at equilibrium,

$$(dG)_{T,P} = 0 \tag{2}$$

a system of N_S in general highly nonlinear algebraic equations is obtained (see e.g. Russel [43]):

$$P_{\langle M\rangle} = \sum_{\nu_A,\cdots,\nu_S=0}^{\infty} \nu_M K^{dis}_{A_{\nu_A}\cdots S_{\nu_S}} \overline{p}^{\left[1-\sum_{i=A}^{S}\nu_i\right]} \prod_{i=A}^{S} P_i^{\nu_i}, \tag{3}$$

where $P_{\langle M\rangle}$ is an assumed overall pressure of element M accruing from all possible dissociative molecular contributions, the indices $\nu_A, \nu_B, \cdots, \nu_S$ respectively are the stoichiometric coefficients of the elements $A, B, C, \cdots, S$ in every molecular species $A_{\nu_A}B_{\nu_B}\cdots S_{\nu_S}$, $\overline{p}$ is again the standard pressure, and $K^{dis}_{A_{\nu_A}B_{\nu_B}\cdots S_{\nu_S}}$ are the dissociation constants for each molecular formation process from the state of completely separated atoms. Thus, the partial pressure of a molecule $A_{\nu_A}B_{\nu_B}\cdots S_{\nu_S}$ is given by:

$$P_{A_{\nu_A}B_{\nu_B}\cdots S_{\nu_S}} = K^{dis}_{A_{\nu_A}B_{\nu_B}\cdots S_{\nu_S}} \overline{p}^{\left[1-\sum_{i=A}^{S}\nu_i\right]} \prod_{i=A}^{S} P_i^{\nu_i} \tag{4}$$

Given $P^{dis} = P_{\langle A\rangle} + P_{\langle B\rangle} + \cdots + P_{\langle S\rangle}$, at a certain temperature e.g. T_0, which fixes the total amount of each atomic species $A, B, \cdots, S$ and all dissociation constants K^{dis}, the system of equations can be solved numerically to yield the equilibrium distribution of partial pressures of all comprised species as a function of temperature. This way to formulate a gas phase equilibrium is consummately general, because any equilibrium constant K of any chemical reaction among the species in the system can be expressed in terms of the constants K^{dis}.

We used the above approach to calculate the gas phase equilibrium of the Al/O system. As there are only two atomic species involved the system (Eq. (3)) consists of just two equations. In the summations only those terms for which the thermochemical data can be found in the literature [6] and the results for the larger Al_xO_y clusters from our present work were included. For sake of completeness the terms for the pure aluminium clusters Al_3 and Al_4 are also incorporated in the sum of equation (3). The corresponding data are given in the appendix. A pressure $P^{dis} = \overline{p} = 1$ bar at $T_0 = 298.15$ K and three different ratios of $\lambda = (P_{\langle Al\rangle}/P_{\langle O\rangle})$, namely $\lambda = (1/300)$, $(1/1)$, and $(300/1)$ were chosen, which represent three different chemical situations. The temperature dependent results are illustrated in Figure 5.

For a large excess of aluminium (i.e. $\lambda \gg 1$) the linearly scaled plot (cf. upper panels) shows, that the most prominent molecular species are the pure Al_x clusters, as expected. Decreasing the temperature they are subsequently formed from Al atoms via Al_2 and Al_3 to Al_4, which is the largest aluminium cluster included in this calculation. The oxygen–rich chemical composition ($\lambda \ll 1$) is dominated by molecular oxygen. Only at high temperatures above $T \approx 2500$ K O_2 is dissociated and therefore its abundance falls off, whereby that of the oxygen atoms is increased. When $\lambda = 1$, i.e. there is oxygen and aluminium equally available, the situation is completely different. In this case $(AlO)_x$ clusters are predominantly present. Especially the tetramer being the largest species enclosed in this study is the dominant aluminium oxide over a wide temperature range. Above approximately $T \approx 2000$ K the tetramer starts decomposing and the smaller $(AlO)_x$ molecules become more abundant. Finally Al_4O_4 disintegrates into the most stable linear aluminium oxide Al_2O and the excessive oxygen can be found as O_2 molecules and O atoms.

The same findings can be inferred from the middle three panels, but as the abundance scale is now logarithmic, the behaviour of the other species in the system becomes discernible. If $\lambda \gg 1$ next to the pure Al_x molecules only Al_xO clusters are abundant and over the whole temperature range Al_2O is the most prevailing aluminium oxide having an about three orders of magnitude higher abundance. In case of $\lambda = 1$ the situation is entirely governed by the aluminium oxides of composition $(AlO)_x$.

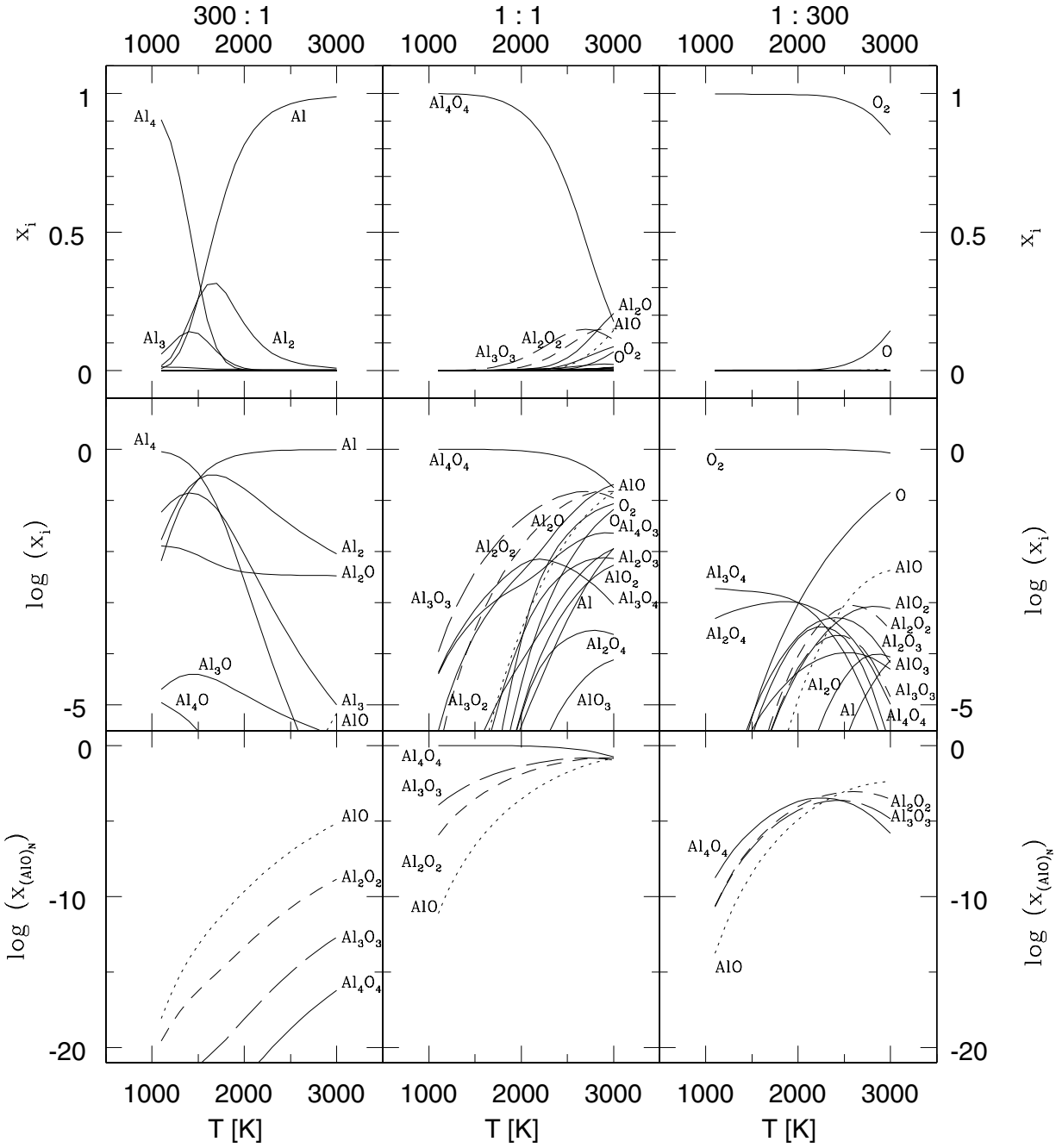

Fig. 5. Abundances $x_i = P_i/P$ for the Al/O system for different stoichiometric ratios λ vs. temperature.

However, also compounds lying on the diagonals adjacent to $(AlO)_x$ are explicitly present. If $\lambda \ll 1$ the behaviour of the aluminium oxide species is much more complex and due to the universal presence of O_2 the abundances of all Al_xO_y species are shifted downwards by about two orders of magnitude in general. At higher temperatures ($T > 2500$ K), except for Al_2O, all important clusters are almost exclusively oxygen–rich. Below 2000 K the two species, Al_2O_4 and Al_3O_4, become dominant. Since Al_3O_4 is the smallest existing $(Al_2O_3)_x$–AlO cluster, these results are in line with the findings of van Heijnsbergen et al. [9], who detected a series of $(Al_2O_3)_x$–AlO clusters with $11 \leq x \leq 71$ produced in a molecular beam by laser vaporisation.

The lower three panels of Figure 5 show in detail the behaviour of the four $(AlO)_x$ species, i.e. those of equal stoichiometric composition. For $\lambda \gg 1$ their abundances increase with rising temperature, whereby AlO is always the most and $(AlO)_4$ the least prominent system. This order is reversed for $\lambda = 1$ over the whole temperature range. When $\lambda \ll 1$ a behaviour like that at $\lambda = 1$ is observed until $T \approx 2200$ K. After this turning point the prominences of the species change their order and the situation resembles again that at $\lambda \gg 1$.

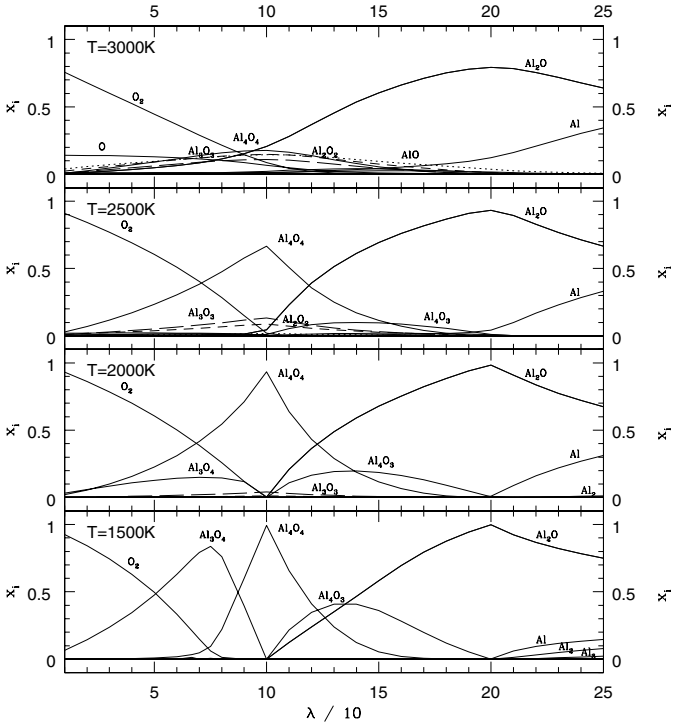

Fig. 6. Abundances x_i for the Al/O system vs. stoichiometric ratios λ at four different temperatures.

To study the conspicuous dependence of the resulting chemical composition on the elemental ratio λ in greater detail Figure 6 shows a different representation of the situation. The abundances x_i are plotted as function of λ for a set of specific temperatures, as can be inferred from the four different panels. Some interesting features become discernible: At all temperatures the system is dominated by O_2 (λ small) and Al_2O (λ large). However, for moderate values of λ (around unity) the development of three additional broad peaks can be observed as the temperature T decreases. These peaks belong to the species Al_3O_4 ($\lambda = 3/4$), Al_4O_4 ($\lambda = 1$), and Al_4O_3 ($\lambda = 4/3$), respectively. In addition, a peak at $\lambda = 2$ can be seen, which is clearly connected to Al_2O, i.e. all peak positions reflect the stoichiometric composition of the corresponding aluminium oxide. All other species, in particular Al_2O_3 having the stoichiometry of the solid, do not seem to be of any importance. However, all these findings depend decisively on the particular species, which are included in the studied chemical system.

5 Summary

For the study of any gas–phase condensation process detailed information about thermodynamic quantities of the relevant molecular species is indispensable. If these quantities are not or just insufficiently at hand from experimental sources, then theoretical techniques are often the only way to obtain the needed data. Consequently, the molecular properties required to set up the thermodynamic functions are here computed for a set of aluminium–oxygen clusters of composition Al_xO_y ($x, y = 1{-}4$) at the DFT/BP86/6–31G(d) level of theory in order to achieve the main objective. Thereby, also the results of AlO_4, Al_4O_2, and Al_4O_3 previously not theoretically investigated are presented in this study.

The thermodynamic functions derived from these DFT results are used to calculate the resulting chemical equilibrium partial pressure distributions for different aluminium and oxygen abundances representing different chemical situations. It is evident, that any equilibrium distribution is strongly influenced by the number and nature of the various species included in the calculation. The present model involves 23 different species with up to eight atoms. According to these chemical equilibrium calculations the temperature dependent formation of small aluminium oxide clusters turns out to be quite sensitive to the aluminium to oxygen ratio.

Table 10. DFT/BP86/6-31G(d) results and related thermochemical properties for the ground states of Al_3 and Al_4.

properties	Al_3	Al_4
state	$^2A_1'$	$^3B_{1g}$
symmetry	D_{3h}	D_{2h}
E_{tot}^{BP86} / Hartree	–727.234882074	–969.678140320
E_{zp} / eV	0.05	0.085
D_{at} / eV	3.85	5.99
r_{12} / Å	2.533	2.578
α_{ijk} /deg	60.0	68.1
$\tilde{\nu}_k$ / cm^{-1}	231 231 350	65 181 214
		298 302 319
$S^{\circ}(T_0)$ / J mol^{-1} K^{-1}	282.1	333.8
$\Delta_f H^{\circ}(T_0)$ / kJ mol^{-1}	615.7	739.8
$\Delta_f G^{\circ}(T_0)$ / kJ mol^{-1}	556.8	674.0

The authors are very grateful to H. Bauer for his achievements in data processing. All calculations were performed on the computers of the Zentrum für Astronomie und Astrophysik (ZAA), TU Berlin, of the Konrad–Zuse–Zentrum für Informationstechnik (ZIB), Berlin, and of the Norddeutscher Verbund für Hoch– und Höchstleistungsrechnen (HLRN).

Appendix

According to Ahlrichs and Elliott [44] the ground states for the Al_3 and Al_4 clusters are a $^2A_1'$ doublet state for a D_{3h} regular triangle and a $^3B_{1g}$ triplet state for a D_{2h} rhombus. The corresponding DFT/BP86/6-31G(d) results and the derived thermochemical data are listed in Table 10.

References

1. H.-P. Gail, E. Sedlmayr, in *The Molecular Astrophysics of Stars and Galaxies*, edited by T.W. Hartquist, D.A. Williams (Oxford Univ. Press, Oxford, 1998), p. 285
2. T. Kozasa, H. Hasegawa, Prog. Theor. Phys. **77**, 1402 (1987)

3. A.G.G.M. Tielens, in *From Miras to Planetary Nebulae: Which Path for Stellar Evolution?*, edited by M.O. Mennessier, A. Omont (Éditions Frontières, Gif-sur-Yvette, 1990), p. 186
4. B. Begemann, J. Dorschner, Th. Henning, H. Mutschke, J. Gürtler, C. Kömpe, R. Nass, Astrophys. J. **476**, 199 (1997)
5. L.R. Nittler, C.M.O.D. Alexander, X. Gao, R.M. Walker, E. Zinner, Astrophys. J. **483**, 475 (1997)
6. M.W. Chase, *NIST-JANAF Thermochemical Tables*, J. Phys. Chem. Ref. Data (American Institute of Physics, New York, 1998), Monograph 9
7. C.B. Alcock, M. Peleg, Trans. Brit. Ceram. Soc. **66**, 217 (1967)
8. H. Yanagida, F.A. Kröger, J. Am. Ceram. Soc. **51**, 700 (1968)
9. D. van Heijnsbergen, K. Demyk, M.A. Duncan, G. Meijer, G. von Helden, Phys. Chem. Chem. Phys. **5**, 2515 (2003)
10. J. Masip, A. Clotet, J.M. Ricart, F. Illas, J. Rubio, Chem. Phys. Lett. **144**, 373 (1988)
11. J. Rubio, J.M. Ricart, F. Illas, J. Comput. Chem. **9**, 836 (1988)
12. A.I. Boldyrev, P.v.R. Schleyer, J. Am. Chem. Soc. **113**, 9045 (1991)
13. E.F. Archibong, R. Sullivan, J. Phys. Chem. **99**, 15830 (1995)
14. H. Wu, X. Li, X.B. Wang, C.F. Ding, L.S. Wang, J. Chem. Phys. **109**, 449 (1998)
15. E.F. Archibong, A. St.-Amant, J. Phys. Chem. A **102**, 6877 (1998)
16. C. Zenouda, P. Blottiau, G. Chambaud, P. Rosmus, J. Molec. Struct. (Theochem) **458**, 61 (1999)
17. T.K. Ghanty, E.R. Davidson, J. Phys. Chem. A **103**, 2867 (1999)
18. T.K. Ghanty, E.R. Davidson, J. Phys. Chem. A **103**, 8985 (1999)
19. M.V. Pak, M.S. Gordon, Chem. Phys. Lett. **344**, 236 (2001)
20. M.T. Swihart, L. Catoire, Combust. Flame **121**, 121 (2000)
21. P. Politzer, P. Lane, M.E. Grice, J. Phys. Chem. A **105**, 7473 (2001)
22. X.-Y. Cui, I. Morrison, J.-G. Han, J. Chem. Phys. **117**, 1077 (2002)
23. A. Martínez, F.J. Tenorio, J. Phys. Chem. A **105**, 8787 (2001)
24. A. Martínez, F.J. Tenorio, J. Phys. Chem. A **105**, 11291 (2001)
25. A. Martínez, L.E. Sansores, R. Salcedo, F.J. Tenorio, J. Phys. Chem. A **106**, 10630 (2002)
26. A. Martínez, F.J. Tenorio, J.V. Ortiz, J. Phys. Chem. A **107**, 2589 (2003)
27. Ch. Chang, A.B.C. Patzer, E. Sedlmayr, D. Sülzle, Eur. Phys. J. D **2**, 57 (1998)
28. Ch. Chang, A.B.C. Patzer, E. Sedlmayr, T. Steinke, D. Sülzle, Chem. Phys. Lett. **324**, 108 (2000)
29. A.D. Becke, Phys. Rev. A **38**, 3098 (1986)
30. J.P. Perdew, Phys. Rev. B **33**, 8822 (1986)
31. J.P. Perdew, Phys. Rev. B **34**, 7406 (1986) (erratum)
32. M.J. Frisch, J.A. Pople, J. S. Binkley, J. Chem. Phys. **80**, 3265 (1984)
33. M.J. Frisch et al., Gaussian98 (Gaussian Inc., Pittsburgh PA, 1998)
34. T.L. Hill, *An Introduction to Statistical Thermodynamics* (Dover, New York, 1986)
35. L. Andrews, T.R. Burkholder, J.T. Yustein, J. Phys. Chem. **96**, 10182 (1992)
36. K.P. Huber, G. Herzberg, *Molecular Spectra and Molecular Structure*, Vol. VI, Constants of Diatomic Molecules (Van Nostrand Reinhold, New York, 1979)
37. I.L. Rozhanskii, L.V. Serebrennikov, V.F. Shevelkov, Khim. Vest. Mosk. Univ. **43**, 560 (1988)
38. M. Cai, C.C. Carter, T.A. Miller, V.E. Bondybey, J. Phys. Chem. **95**, 73 (1991)
39. M.A. Douglas, R.H. Hauge, J.L. Margrave, High Temp. Sci. **16**, 35 (1983)
40. S.R. Desai, H. Wu, C.M. Rohlfing, L.-S. Wang, J. Phys. Chem. **106**, 1309 (1997)
41. S.G. Lias, J.E. Bartmess, J.F. Liebman, J.L. Holmes, R.D. Levin, W.G. Mallard, J. Phys. Chem. Ref. Data **17**(Suppl. 1), 41 (1988)
42. M. Binnewies, E. Milke, *Thermochemical Data of Elements and Compounds* (Wiley–VCH, Weinheim, 1999)
43. H.N. Russell, Astrophys. J. **79**, 317 (1934)
44. R. Ahlrichs, S.D. Elliott, Phys. Chem. Chem. Phys. **1**, 13 (1999)